High-field diffusion tensor imaging characterization of cerebral white matter injury in LPS exposed fetal sheep

Yohan van de Looij[1,2], Gregory A Lodygensky[1], Justin M Dean[3], Henrik Hagberg[3], Carina Mallard[3], Petra S Hüppi[1], Rolf Gruetter[2,4], and Stéphane Sizonenko[1]

[1]Division of Child Growth & Development, University of Geneva, Geneva, Switzerland, [2]Laboratory for Functional and Metabolic Imaging, Ecole Polytechnique Fédérale de Lausanne, Lausanne, Switzerland, [3]Perinatal Center, University of Gothenburg, Göteborg, Sweden, [4]Department of Radiology, University of Geneva and Lausanne, Geneva and Lausanne, Switzerland

Introduction:

Encephalopathy of prematurity, characterized by focal and diffuse white matter (WM) injuries, is a major cause of developmental disabilities in up to 75% infants after preterm birth. In those infants, hypoxemia and inflammation are the two main causes of WM damage. As such, inflammatory brain injury model can be achieved by bacteria-derived lipopolysaccharide (LPS) exposure. Nevertheless, in gyrencephalic species such as sheep, precise anatomical and microstructural characterization of the consequences of fetal inflammation remains scarce but could be interesting for the comprehension of mechanisms of perinatal brain injury. The aim of this study was to provide MRI delineation of the changes in the developing WM following LPS exposure in the 0.7 gestation fetal sheep (corresponding to human preterm at 28-32 weeks of gestation). Multimodal MRI techniques were performed: T_1W, T_2W images and Diffusion Tensor Imaging (DTI). The changes in MRI and DTI derived parameters in the common lesions seen in premature humans were characterized and correlated to histopathology.

Material and Methods:

Fetal sheep at 103d of gestation (term = 145d) received vehicle (Sham, n=9) or LPS (200ng; n=9). Fetal brains were collected after 10d recovery and formalin-fixed for subsequent *ex-vivo* MRI. T_1 and T_2W images were acquired on a 3T Siemens Trio System with a standard wrist coil. T_1W images were acquired with MPRAGE sequence (inversion time = 600 ms, TE = 3.17 ms and flip angle = 8°) and T_2W with a Turbo Spin Echo sequence (TR = 4910 ms, TE = 141 ms, flip angle = 150°, echo train length = 15). DTI experiments were performed on an actively-shielded 9.4T/31cm magnet (Varian/Magnex) with a custom build solenoid 50-mm RF coil. Scans were averaged 2 times with TE/TR = 35/11000 ms, a resolution of 0.19×0.19×1 mm^3 and a *b*-value set to 1971 $s.mm^{-2}$. Quantitative measurements of cerebral tissue volumes (gray matter (GM), basal ganglia (BG), white matter (WM) and nonliving liquid) were performed using a nonparametric signal intensity estimator with k-nearest neighbor (*kNN*) classification [1]. Manual delineation of region of interest (ROI) was achieved on Direction Encoded Color (DEC) maps and radial ($D_\perp$), axial ($D_{//}$), mean (MD) diffusivities and fractional anisotropy (FA) were derived from the tensor using homemade Matlab (Mathworks, Natick, MA) software. Free software, *MedInria DTI track* was used for the computation and the display of the principal eigenvectors. The corpus callosum (CC) thickness was manually measured on DEC maps with ImageJ. Three different patterns of signal abnormalities were recognized on anatomical MR images: hypersignal T_2 and hyposignal T_1 (focal and diffuse) as well as hyposignal T_2 and hypersignal T_1 (focal only). For each of these injured animals, a ROI was manually delineated in the lesion on the corresponding T_2W image and DTI derived parameters were averaged in the lesion. Following MRI, coronal sections were collected and stained with acid fuchsin/thionin (AF/T), immunohistochemically to detect astrocytes (anti-mouse GFAP, 1:250, Sigma), neurofilament (monoclonal anti-phos-Neurofilaments, SMI312, 1:2000, Covance), and amyloid precursor protein (mouse anti-Alzheimer precursor protein A4, 1:100, Millipore). Statistical significance (P<0.05) was achieved with a Mann-Whitney test.

Results and discussion:

Total brain volume (i.e., WM+GM+BG) (Sham group: 21.9 ± 1.4 ml, LPS group: 20.3 ± 1.7 ml; P=0.02), WM volume (Sham group: 10.5 ± 1.2 ml, LPS group: 9.2 ± 1.0 ml; P=0.02) as well as CC thickness (Sham group: 3.2 ± 0.9 mm, LPS group: 2.1 ± 0.6 mm; P=0.004) were significantly lower in the LPS group compared with Sham group. These changes can be related to an altered growth of the brain comparable to human preterm infants with white matter injury [2]. In the CC and in the periventricular WM (PVWM), FA values were significantly lower in the LPS group than in the Sham group (CC: 0.78 ± 0.04 vs. 0.64 ± 0.06; PVWM: 0.66 ± 0.07 vs. 0.49 ± 0.09; P<0.01), principally due to an increase of $D_\perp$. This $D_\perp$ increased has been attributed to a loss of myelin in adult animal models [3] but at the developmental stage used in this study, WM myelination has just begun. As such, changes in $D_\perp$ are likely to represent a more global white matter structure disruption. Of note, several MR studies in preterm infants with WM injury exhibited similar results [4]. Diffuse WM lesions in the intragyral WM were identified (hyposignal T_1, hypersignal T_2, low FA due to increased $D_\perp$). These lesions demonstrated marked alteration in AF/T staining on histology with reduced cellularity, no change in GFAP-astrocytes and evidence of reduced NF- and APP-positive cells. These lesions show the same properties as the diffuse white matter hyperintensity (Diffuse Excessive High Signal Intensity-DEHSI) well described in human premature infants [5]. Focal "necrotic" lesions were observed in the fronto-parietal PVWM (hypersignal T_1, hyposignal T_2, FA close to the one of GM due to increased $D_\perp$). These regions exhibited disorganization of the fibers depicted by a moderately altered pattern of the eigenvectors (Fig.1 - *Necrotic lesion*). On histology, areas with lesion identified as "necrotic" by MRI demonstrated a cell necrosis pattern seen on AF/T and involving all cellular elements with neuronal APP accumulation, NF and GFAP loss (Fig. 1). These lesions exhibit similar location, anatomy and microstructure to the punctate lesions often observed in human premature infants [6]. Typical "cystic" lesions of periventricular leukomalacia were also detected, characterized by very strong hyposignal T_1, hypersignal T_2, very high MD and $D_\perp$ resulting in FA values comparable to the one of CSF as well as a large disruption of WM fibers at the lesion site depicted by the absence of diffusion eigenvectors (Fig. 1 - *Cystic lesion*). Periventricular cysts and similar disruption of white matter tracts are a hallmark of cystic periventricular leukomalacia seen in preterm infants leading to significant motor visual and cognitive impairment [7].

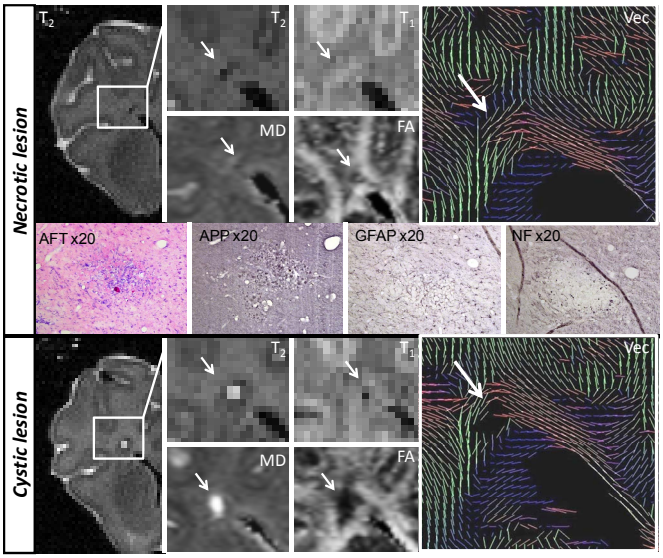

Fig. 1: *T_2W (T_2), T_1W (T_1) images, MD, FA maps and DEC maps of the eigenvectors (Vec) zoomed on the lesions of a typical LPS sheep brain. Main changes (arrows): up panel, necrotic lesion: hypersignal T_1, hyposignal T_2, low MD, FA close to GM and moderate disruption of the fibers at the lesion site. In the "necrosis" (middle panel): loss of GFAP, NF and accumulation of APP. Low panel, cystic lesion: strong hyposignal T_1 and hypersignal T_2, very high MD and FA close to CSF; no fiber at the lesion site.*

Conclusion:

The combination of lesions depicted by DTI in LPS treated fetal sheep (i.e. DEHSI, punctate lesions and cysts) mimics very well the pattern of injuries seen in premature infants confirming the relevance of such a model. More specifically, we show the excellent ability of DTI to classify different types of brain lesions following LPS exposure with specific changes of DTI derived parameters as well as of the eigenvectors tracking between cysts and necrotic lesions. By characterizing the effects of a fetal inflammatory brain injury with MRI and DTI, this study establishes the groundwork necessary for better understanding of clinical MRI of preterm encephalopathy and for the evaluation of future neuroprotective strategies.

References: [1] Hüppi PS. Ann Neurol 1998; [2] Nosarti C. Hum Brain Mapp 2011; [3] Song SK. Neuroimage 2002; [4] Hüppi PS. Ped Res 1998; [5] Maalouf EF. J Pediatr 1999; [6] Rutherford MA. Neuroradiology 2010; [7] Ramenghi LA. Early Hum Dev 2009.

Acknowledgements: Supported by the Fond National Suisse (° 31003A-112233 and SPUM N°33CM30-124101), NEOBRAIN Consortium, European Commission, the Centre d'Imagerie Biomédicale (CIBM) of the UNIL, UNIGE, HUG, CHUV, EPFL, the Leenards and Jeantet Foundation.